

# Numerical construction of quasi-invariants in double- and multi-bend achromat lattices

Yongjun Li,<sup>1,\*</sup> Kilean Hwang,<sup>2</sup> Chad Mitchell,<sup>2</sup> Robert Rainer,<sup>1</sup> Robert Ryne,<sup>2</sup> and Victor Smaluk<sup>1</sup>

<sup>1</sup>*Brookhaven National Laboratory, Upton, New York 11973, USA*

<sup>2</sup>*Lawrence Berkeley National Laboratory, Berkeley 94720, California, USA*

A numerical method to construct quasi-invariants (QI) has been explored in double- and multi-bend achromat (DBA and MBA) lattices. The Fermilab's Integrable Optics Test Accelerator (IOTA) and the University of Maryland Electron Ring (UMER) built with exact invariants, pave the way for discovery of a new type of nonlinear lattice. But it might be impossible to construct exact invariants in various achromatic lattices for dedicated synchrotron light source storage rings. Quasi-invariants, however, were found to be constructible by tuning the sextupoles and octupoles in the DBA and MBA lattices. In our exploration, QIs were constructed by confining the simulated trajectories to tori in the phase space at a certain Poincaré section, while simultaneously maintaining monochromatic betatron tunes. The lattices with QIs share some important features as integrable ones, such as a large dynamic aperture, confined trajectory tori, robustness to resonances and errors, and a large amplitude-dependent tune-spread.

## I. INTRODUCTION

The Integrable Optics Test Accelerator (IOTA) [1] and University of Maryland Electron (UMER) [2] constructed with one or more exact invariants [3, 4], paves the way for discovery of a new type of nonlinear lattice. To be integrable, however, imposes strong constraints on the linear optics pattern in order to accommodate special nonlinear magnetic inserts. The storage rings used as dedicated synchrotron light sources, are designed in a different way: a linear achromat lattice with a desired beam emittance is designed first; then nonlinear dynamics is optimized with sextupoles and/or octupoles. These nonlinear magnets usually control the low order resonance driving terms of the single-turn Hamiltonian [5] to obtain sufficient dynamic apertures (DA). Under these conditions it is generally difficult, if not completely impossible, to construct exact invariants on those rings. Quasi-invariants (QI), however, were found to be constructible in the achromat lattices. This paper introduces

our exploration into numerically constructing and applying such QI in both double-bend achromat (DBA) and multi-bend achromat (MBA) lattices. The motivation for constructing such lattices is that, although they are not completely integrable, particle motion within their DA are much less chaotic and more robust to the resonances. Lattices such as the one seen at the IOTA, usually have a large amplitude-dependent betatron tune-spread which can increase instability and space charge thresholds due to improved Landau damping. This research was also motivated by related studies such as the square matrix method [6] and constant Courant-Snyder variants method [7, 8].

To further explain our approach, the remaining sections are outlined as follows: Sect. II explains the conception of Poisson commuting invariants in integrable Hamiltonian systems, and the numerical approach of constructing linear [action-angle]-like QIs through the symplectic tracking simulations. Sect. III and IV introduce the nonlinear properties of two constructed nonlinear lattices respectively: the existing NSLS-II DBA lattice ring, and an under-designed diffraction-limited MBA lattice

---

\* Email: yli@bnl.gov

ring. Some detailed studies focusing on the DBA lattice are then further explained: a technique to modulate the action-like variant to reshape the tori is illustrated in Sect. V; a simulation of the kicked beam decoherence to observe the large nonlinear tune-spread is shown in Sect. VII; The periodicity of QI is introduced in Sect. VI. Some discussion and a brief summary are given in Sect. VIII.

## II. NUMERICAL CONSTRUCTION OF QUASI-INVARIANTS

The Liouville integrability of a Hamiltonian system means there exists a maximal set of Poisson commuting invariants, i.e., functions on the phase space whose Poisson brackets with the Hamiltonian of the system and with each other, vanish [9, 10]. Systems with these conditions are completely integrable, distinguishing them from partial integrable systems by having less invariants. By ignoring radiation and longitudinal acceleration, a charged particle's transverse motion in a storage ring is a 4-dimensional Hamiltonian system. If we let the canonical coordinates of the system be  $\mathbf{z} = (x, p_x; y, p_y)$ , and its single-turn Hamiltonian be  $H$ , the free variable is the path length of the reference particle  $s = n \times C$ , where  $n = 1, 2, \dots$ , and  $C$  is the circumference of a ring. For any function  $f(s, \mathbf{z})$ , its value changes with  $s$  either because of its explicit  $s$  dependence, or because it depends on  $\mathbf{z}$  and changes because  $\mathbf{z}$  changes. The total derivative of  $f$  therefore can be written as

$$f' = \frac{\partial f}{\partial s} + [f, H],$$

where  $[\cdot, \cdot]$  is the Poisson bracket. A quantity  $f(\mathbf{z})$  is a constant of the motion if it is not explicitly  $s$  dependent, and satisfies the condition

$$[f, H] = 0.$$

If four such independent invariants  $f_i$  with  $i = 1, 2, 3, 4$  exist and they commute with each other,

$$[f_i, f_j] = 0,$$

i.e., any two of them form a pair of Poisson commuting set, the lattice is completely Liouville integrable. In the linear beam dynamics, uncoupled action-angle variables  $J_x - \phi_x$ ;  $J_y - \phi_y$  are the most common used Poisson commuting pairs.

In the existing, conventional storage rings (i.e., non-IOTA type), various linear magnets are used to achieve desirable linear optics properties, e.g., a low beam emittance. Once the linear lattice and the nonlinear magnets locations are fixed, the single-turn Hamiltonian  $H$  is the function of the coordinates  $\mathbf{z}$  and the nonlinear magnet's excitations  $K_i$ , with  $i \geq 2$ . It is difficult, if not impossible, to construct even one exact invariant in the conventional storage rings. However, the topology of trajectories observed at a Poincaré section for a completely integrable system is well-known, i.e., all its trajectories are confined to tori with well-defined and stable tunes. The Poincaré section is the intersection of a periodic orbit in the state space of a continuous dynamical system with a certain lower-dimensional subspace, which is transverse to the flow of the system. When only linear magnets are present, the linear action-angle variables  $J - \phi$  are a pair of commuting invariants, and  $\phi$  is constant regardless of the betatron amplitude. Based on this picture, we can imitate the linear motion to construct a pair of QIs as illustrated in Fig. 1. Unlike the linear case, however, the angle variant can be dependent on the amplitude of actions.

The uncoupled action-like variant in the quadratic form is constructed as

$$J_x^2(x, p_x) = \bar{x}^2 + \bar{p}_x^2 = \gamma_x x^2 + 2\alpha_x x p_x + \beta_x p_x^2, \quad (1)$$

in the horizontal plane. Here the normalized coordinates  $\bar{x}$  and  $\bar{p}_x$  are read as

$$\begin{bmatrix} \bar{x} \\ \bar{p}_x \end{bmatrix} = \begin{bmatrix} \frac{1}{\sqrt{\beta_x}} & 0 \\ \frac{\alpha_x}{\sqrt{\beta_x}} & \sqrt{\beta_x} \end{bmatrix} \begin{bmatrix} x \\ p_x \end{bmatrix}. \quad (2)$$

Here  $\alpha_x$ ,  $\beta_x$ , and  $\gamma_x$  are the horizontal Twiss parameters [11] at a given longitudinal location, where the Poincaré section is observed.

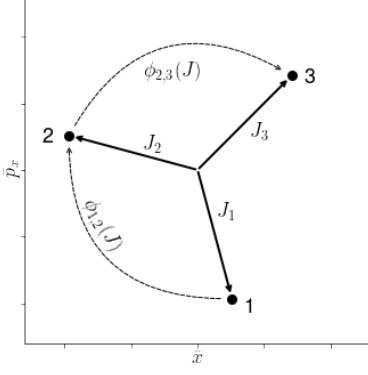


Figure 1. Schematic illustration of a rotating trajectory observed at a Poincaré section with normalized coordinates  $(\bar{x}, \bar{p}_x)$ . The fluctuations of action  $J$  and phase advances  $\phi$  in multiple-turn tracking simulations are the objectives to be minimized.

The variant  $\phi_x$  corresponds to the phase advance completed in a single revolution, and is constructed as

$$\begin{aligned}\phi_x &= \Phi_{x,i+1} - \Phi_{x,i} \\ &= \arctan\left(\frac{\bar{p}_{x,i+1}}{\bar{x}_{i+1}}\right) - \arctan\left(\frac{\bar{p}_{x,i}}{\bar{x}_i}\right) + k \cdot 2\pi,\end{aligned}$$

where  $k$  is the integer part of betatron tune.

With a given one-turn Hamiltonian  $H(K_i, x, p_x, y, p_y)$ , by tuning its nonlinear knobs  $K_i$ , one can minimize their absolute derivative expressed by the Poisson bracket

$$\begin{cases} \min_{K_i} |J_x(x, p_x), H(K_i, x, p_x, y, p_y)| \rightarrow 0 \\ \min_{K_i} |\phi_x(x, p_x), H(K_i, x, p_x, y, p_y)| \rightarrow 0 \end{cases}, \quad (3)$$

at different coordinates  $(x, p_x; y, p_y)$ .

In order to compute the Poisson brackets in Eq. (3), we need to extract the single-turn Hamiltonian  $H$  explicitly. For a given ring lattice, each magnet has its own Lie generator, and the whole ring's single-turn Hamiltonian can be obtained by concatenating these Lie generators sequentially [5]. An alternative is to reconstruct the Hamiltonian from the single-turn Taylor map [12] obtained with the truncated power series algorithm (TPSA) [13]. The Hamiltonians obtained with the above two techniques are still approximate because one must truncate the maps at a certain order. In principle, one can use an

approximate Hamiltonian to calculate the derivative of a function  $f$  with the Poisson bracket, but it is needed to estimate and control the accuracy carefully. Therefore, instead of using an approximate Hamiltonian to compute the Poisson brackets, we implemented element-by-element tracking from given initial conditions to compute the turn-by-turn evolution of  $J_x$ . The tracking was implemented with a kick-drift symplectic integrator [14]. The reason for using symplectic integrator is to preserve the geometry of the Hamiltonian system. To ensure the actions  $J_x$  are QIs from different initial conditions within the needed DA, multiple particles with different  $J_{x,0}$  were launched. The available nonlinear knobs were simultaneously tuned to minimize turn-by-turn fluctuations as illustrated in Fig. 2.

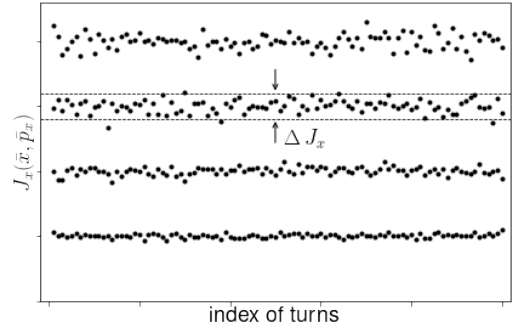


Figure 2. Schematic illustration of the fluctuation of actions  $\Delta J_x$  starting from different initial amplitudes. Usually the fluctuations increase gradually with the initial amplitude.

Confining the fluctuation of the angle variant  $\phi_x$  is equivalent to maintaining a monochromatic betatron tune. Instead of directly calculating the fluctuation of phase advances, turn-by-turn complex eigenmodes  $\bar{x} \pm i\bar{p}_x$  [15] was analyzed in the frequency domain. The reason for using the eigenmodes here is to determine if the fractional tune is below or above the half integer. The amplitudes of two leading harmonics were computed utilizing the Numerical Analysis of Fundamental Frequencies (NAFF) technique [16]. By tuning the nonlinear knobs, the ratio between the two leading harmonics  $r = \frac{A_2}{A_1}$  is suppressed, as well as with other, smaller am-

plitude harmonics as illustrated in Fig. 3. Note that here we only require that the tune for each initial condition be monochromatic, but allow it to be amplitude dependent as well. In the same way, another pair of QIs ( $J_y - \phi_y$ ) can be constructed in the vertical plane.

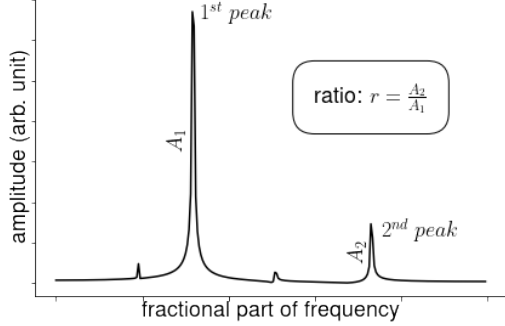


Figure 3. Schematic illustration of the spectrum analysis with the turn-by-turn trajectory data  $\bar{x} \pm i\bar{p}_x$ . The ratio between two leading harmonics amplitudes  $\frac{A_2}{A_1}$  is the minimization objective in order to obtain monochromatic tune.

Since we want to minimize the fluctuations of four different variants with different initial conditions simultaneously, the construction of such a nonlinear lattice becomes a typical multi-objective (MO) optimization problem:

- given a set of nonlinear knobs  $K_i$  within their allowed ranges;
- subject to some constraints, such as certain desired chromaticities;
- simultaneously minimize the objective functions, i.e.,  $\frac{\Delta J_{x,y}}{J_{x,y}}$  and  $r_{x,y}$  of multi-particles launched from different initial conditions.

The MO optimization techniques are widely used in the accelerator community now, and more details can be found in [17].

Thus far, we have only discussed uncoupled linear lattices. When linear coupling is present, a parameterization, such as the one depicted in ref. [18], is needed.

### III. APPLIED TO DOUBLE-BEND ACHROMAT

In this Section, we introduce a constructed nonlinear DBA lattice for the NSLS-II main storage ring. NSLS-II [19] is a dedicated 3<sup>rd</sup> generation medium energy (3 GeV) light source operated by Brookhaven National Laboratory. The storage ring's lattice is a typical DBA structure with main parameters listed in Table I. Its linear optics for one cell is illustrated in Fig. 4. The whole ring is composed of 30 such cells. In this configuration, three families of chromatic sextupoles are used to correct its chromaticity to +7. Then six families of harmonic sextupoles in dispersion-free sections are the tuning knobs for the multi-objective optimizer to construct four QIs.

Table I. Main parameters of NSLS-II storage ring

Parameters	Values
Hor. emit. (nm)	2.1
Natural chrom. (x/y)	-101/-40
Tune (x/y)	33.22/16.26
Energy spread	$5.1 \times 10^{-4}$
Damp. partition (x/y/s)	1.0/1.0/2.0

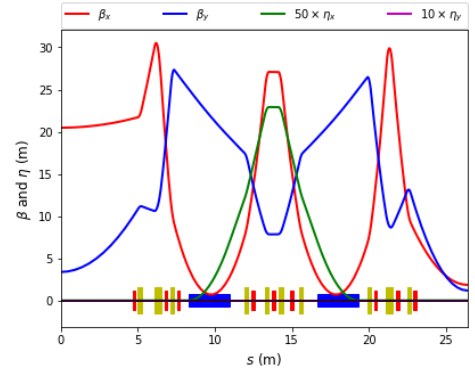


Figure 4. (Colored) The linear optics and magnet layout for one cell of the NSLS-II storage ring. The red blocks represent sextupoles. Six harmonic sextupoles were used in searching QIs.

Below we present the nonlinear lattice performance of an optimized solution using the tracking simulation code ELEGANT [20]. All the tracking simulations in this paper

were implemented with this code unless stated otherwise. First a sufficient on-momentum DA (through 1,024 turns particle tracking) has been confirmed as shown in Fig. 5. Each stable initial condition is also colored with the tune diffusion rate obtained with the NAFF technique.

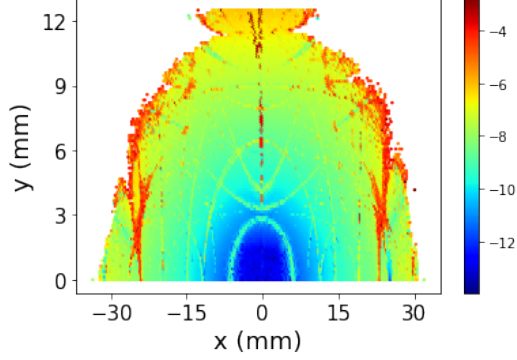


Figure 5. (Colored) DA of the DBA lattice observed at the center of long straight section, i.e.,  $s = 0$  in Fig. 4. It was colored with the tune diffusion rate.

The fluctuations of action  $J_{x,y}$  at different amplitudes are illustrated in Fig. 6. The fluctuation increases gradually with the amplitude of initial condition. The spectrum analysis using the NAFF technique indicates that some harmonics gradually become stronger as well (Fig. 7). The amplitude ratios between two leading harmonics increase as shown in Fig. 8.

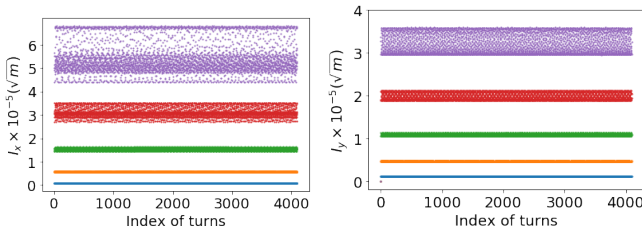


Figure 6. (Colored) Fluctuation of  $J_{x,y}$  of the DBA lattice starting from different initial conditions in the horizontal (left) and vertical (right) planes.

One of the features of an integrable system is that the trajectories are confined to tori in the phase space, which are shown in Fig. 9. Although trajectories begin to deviate from the desired ellipse gradually when the amplitude

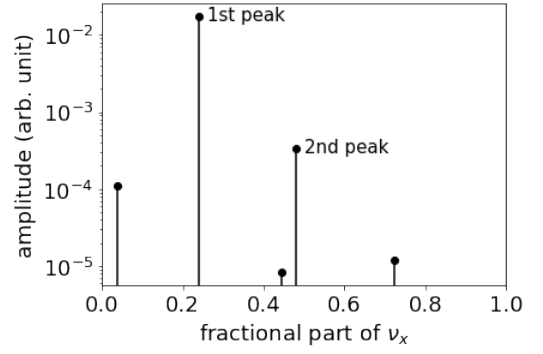


Figure 7. Some leading harmonics extracted from a set of turn-by-turn data  $\bar{x} \pm i\bar{p}_x$  using the NAFF technique for the DBA lattice. Only the first two leading harmonics ratio is used for the minimization objective .

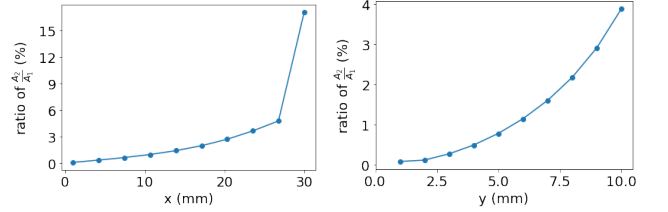


Figure 8. Ratio of two leading harmonics amplitudes gradually increases with the initial amplitude in the horizontal (left) and vertical (right) planes for the DBA lattice.

increases, they are still confined to their own tori. It indicates some high order terms might be needed in order to construct a better QI in Eq. (1).

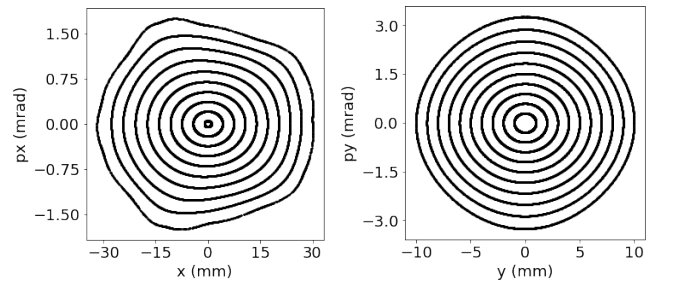


Figure 9. Simulated trajectories of the DBA lattice starting from different initial conditions in the horizontal (left) and vertical (right) phase space. Within the DA, although the trajectories deviate from desired circles gradually, they are still confined to thin tori.

Like the IOTA rings, this lattice also provides a

large amplitude-dependent tune-spread as illustrated in Fig. 10. This property can increase instability and space charge thresholds through an improved Landau damping effect.

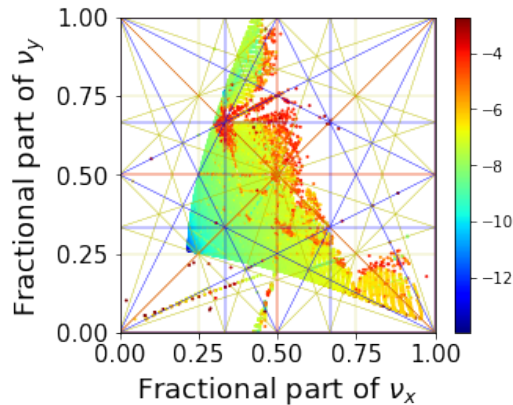


Figure 10. (Colored) Tune footprint of the DBA lattice in the tune space. A large amplitude-dependent tune-spread is observed, and various resonance lines can be crossed.

The robustness of this lattice has been confirmed in both the simulation and experiment. After adding various realistic errors to the magnets in the simulation, a sufficient DA still remains. Experimentally this lattice had been successfully commissioned at NSLS-II. Comparing with the current operation sextupole configuration, under a same condition of 400 mA stored beam current, the needed bunch-by-bunch feedback amplitude gain could be reduced by 50% and 75% in the horizontal and vertical planes respectively thanks to the larger chromaticity and nonlinear tune-spread.

#### IV. APPLIED TO MULTI-BEND ACHROMAT

Now the low emittance light source ring design is entering a new era. Various MBA-type lattices already reach diffraction-limited horizontal emittances to deliver much brighter X-ray beams. It is interesting to explore if it is possible to construct some QIs in the MBA lattice as well. The ESRF-EBS type hybrid MBA lattice [21] has been widely adopted by other facilities. It is also being con-

sidered as one of options for the future NSLS-II upgrade. An underdesigned 7-BA lattice's linear optics for one cell is illustrated in Fig. 11, in which several reverse bends are incorporated [22, 23] as well. The main parameters are listed in Table II.

Table II. Main parameters of the test hybrid MBA ring

Parameters	Values
Hor. emit. ( $pm$ )	31
Natural chrom. ( $x/y$ )	-125/-108
Tune ( $x/y$ )	73.19/28.62
Energy spread	$7.1 \times 10^{-4}$
Damp. partition ( $x/y/s$ )	2.0/1.0/1.0

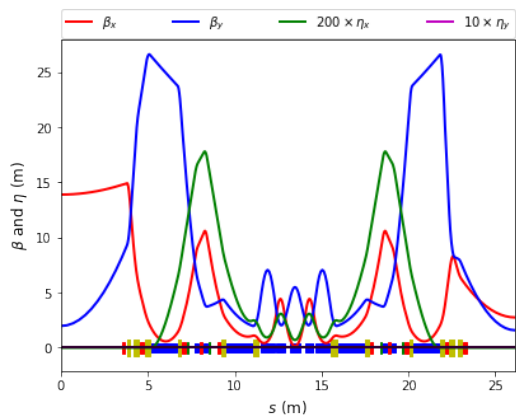


Figure 11. (Colored) The linear optics and magnet layout for one cell of an ESRF-EBS type hybrid 7BA lattice. The red blocks represent sextupoles. Six chromatic sextupoles grouped into five families inside two dispersive bumps are used to correct the chromaticity with three extra degrees of freedom. Four harmonic sextupoles and four dispersive octupoles (green blocks) are also available for nonlinear dynamics optimization.

A two-stage optimization has been implemented. First, both chromatic and harmonic sextupoles were used to correct chromaticities and minimize the fluctuations of the QIs. Then four octupoles inside the dispersive bumps were used to further minimize their residual fluctuations. A sufficient DA is obtained as shown in Fig. 12.

The MBA lattice is found more challenging than the

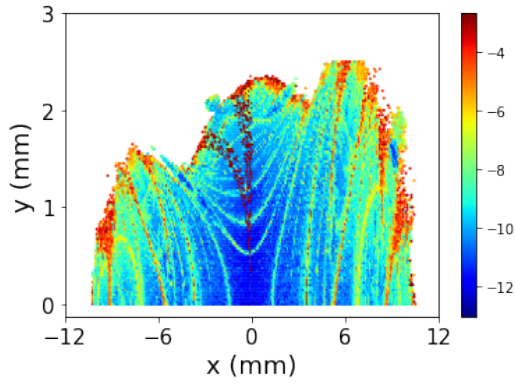


Figure 12. (Colored) DA of the MBA lattice in the transverse  $x - y$  plane colored with the tune diffusion rate.

DBA lattice in constructing QIs. The constructed QIs have larger fluctuations, especially in the vertical plane as illustrated in Fig. 13 and 14. Nevertheless, their trajectories are still confined to tori in the horizontal plane as seen in Fig. 15. More importantly, a large amplitude spread is also observed in its tune footprint as shown in Fig. 16.

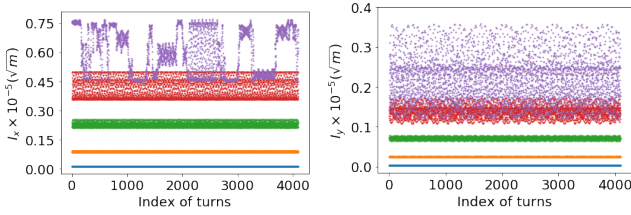


Figure 13. (Colored) Fluctuation of  $J_{x,y}$  of the MBA lattice in the the horizontal (left) and vertical (right) planes.

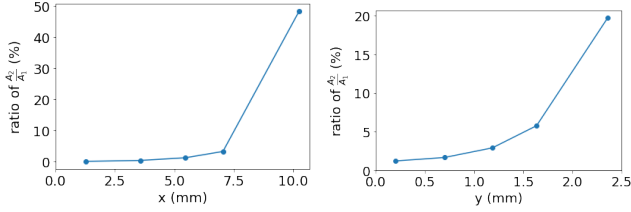


Figure 14. Ratio of two leading harmonics amplitude of the MBA lattice in the the horizontal (left) and vertical (right) planes.

While observing the trajectories of the vertical phase space in Fig. 15, at a large amplitude, they significantly

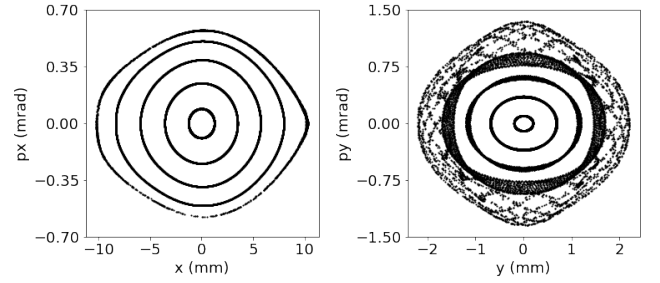


Figure 15. Simulated trajectories of the MBA lattice in the horizontal (left) and vertical (right) phase space. The vertical trajectories begin to smear out from thin tori gradually, but some patterns are visible.

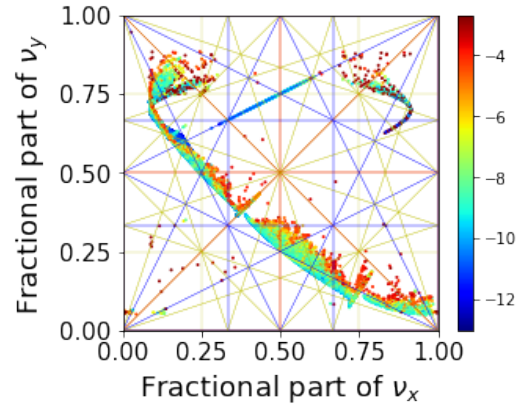


Figure 16. (Colored) A large amplitude-dependent tune-spread is observed in the MBA lattice constructed with QIs.

deviate from our desired shape, but regular patterns can be recognized. That means the motion is still regular rather than chaotic, but a complicated QI expression including high order polynomial terms are needed. Thus far it is clear for us how to construct better QIs analytically.

## V. MODULATION ON QUASI-INVARIANT

An exact invariant of nonlinear integrable Hamiltonian system couldn't be in a simple quadratic form as we constructed. We can add extra high order polynomial terms to construct more complicated quasi-variant. In this section, we demonstrate an alternative method by periodically modulating the quasi-invariant  $J_x$  to obtain



triangle-shaped tori,

$$\begin{aligned} J(\phi_x) &= J_0 + \Delta J_x(\phi_x) \\ &= J_0 \left\{ 1 + \delta \sin \left[ n \left( \phi_x - \frac{\pi}{2n} \right) \right] \right\}, \end{aligned} \quad (4)$$

where  $\delta = \frac{\Delta J_x}{J_x}$  and  $n = 3$ . The modulation (top) on  $J_x$  and the expected torus are illustrated in Fig. 17,

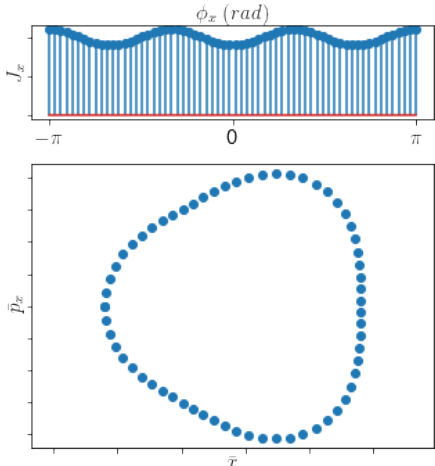


Figure 17. (Colored) A azimuthal periodical modulation (top) on the action QI can reshape a circle torus into a triangle-shaped one (bottom).

Applying the above modulation into the optimization objectives in the DBA lattice, a new set of sextupole settings were obtained. A tracking simulation confirmed that the tori have been reshaped as expected in Fig. 18. Such phase space manipulation technique might be useful when a non-symmetric DA is desired. For example, a slightly larger inboard DA is preferred to capture off-axis injected beam from there.

This modulation could introduce some weak harmonics into the betatron spectrum. For example, a weak harmonic sitting near  $1/3$  is visible through the NAFF analysis in Fig. 19. Because the modulation amplitude is usually weak, it usually doesn't spoil the overall performance of the nonlinear lattice. Note that the triangle-shaped tori are not caused by the betatron tune's approaching to a third-order resonance. As seen in Fig. 19, the main betatron tune is around 0.22, and still far away

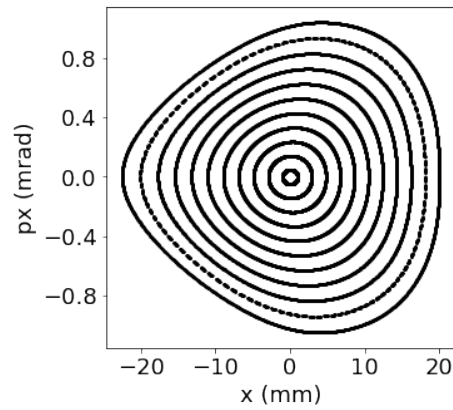


Figure 18. Particle trajectories are confined to triangle-shaped tori as confirmed by the tracking simulation. Usually a non-symmetric DA can be obtained with this modulation technique.

from  $1/3$ .

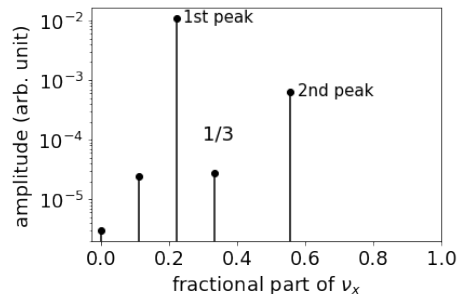


Figure 19. A weak  $1/3$  harmonic is visible when a triangle-shaped modulation is added on a torus. The dominated tune is still around 0.22. The tori are modulated as triangle shapes but not because the main tune is approaching the third order resonance.

## VI. PERIODICITY OF QUASI-INVARIANTS

In our examples, the QIs were constructed at a specific Poincaré section, e.g., at the center of straight section in our examples. Therefore it is not surprised to observe distorted tori at other locations. An example of distorted tori observed at a location inside the achromat of the NSLS-II DBA lattice is illustrated in Fig. 20. The one-cell map behaves like an “optical anastigmat”, which



has regular tori only at the periodical locations, i.e., its entrance and exit. But distorted tori, even the chaos can be observed somewhere in-between.

## VII. DECOHERENCE DUE TO NONLINEARITY

The amplitude-dependent tune-spread due to the nonlinearity of betatron oscillation can be observed by kicking a bunched beam transversely [24]. A 4-dimensional multi-particle simulation was used to confirm it. After being kicked, the beam motion will decohere as the individual betatron phases of the particles disperse. The phase space distribution of the beam spreads from a localized bunch to an annulus which occupies all betatron phases (see Fig. 21), and the observed centroid of the beam will show a decaying oscillation (see Fig. 22). From the decoherence factor curve (the red line in Fig. 22), the local tune-shift-with-amplitude coefficient can be determined, and confirmed with the spectrum analysis of the single particle tracking data in Fig. 23.

## VIII. DISCUSSION AND SUMMARY

Thus far, we only studied the on-momentum particle motion. Practically a sufficient off-momentum acceptance is required as well. In the two examples shown previously, only the on-momentum lattice were constructed with four quasi-variants, then the off-momentum acceptances were checked with tracking simulation. They were found already having sufficient momentum acceptance. In case the momentum acceptance needs to be

optimized simultaneously, we expanded the method to include fixed off-momentum particles. For a fixed off-momentum particle, its dispersive reference orbit needs to be computed first, and then its action-like variants are constructed with the momentum-dependent Twiss parameters  $\alpha(\delta, K_i)$ ,  $\beta(\delta, K_i)$  and  $\gamma(\delta, K_i)$  in Eq. (2). The momentum-dependent Twiss parameters also depend on the nonlinear magnets excitations. For a given nonlinear magnet setting, the reference closed orbit and corresponding momentum-dependent Twiss parameters need to be updated prior to the normalization.

We demonstrated that a quadratic form of the action- and angle-like QIs are constructible in the conventional DBA and MBA lattices by tuning conventional sextupoles and octupoles. The obtained QIs are only valid within a limited DA. However, most particles trajectories are regular and confined to tori, their betatron tunes are well-defined and stable. As real IOTA-type lattice, a large nonlinear tune-spread also exists, which can provide extra Landau damping.

## ACKNOWLEDGMENTS

We would like to thank L-H. Yu (BNL), M. Borland, R. Lindberg, Y. Sun (ANL) and Y. Hao (MSU), E. Stern, A. Valishev, A. Romanov (FNAL), N. Kuklev (UChicago), G. Xu (IHEP) for the stimulating and collaborative discussions. This research is supported by the U.S. Department of Energy under Contract No. DE-SC0012704 (BNL) and DE-AC02-05CH11231 (LBNL). Co-authors from LBNL would like to acknowledge the support from the U.S. DOE Early Career Research Program under the Office of High Energy Physics.

---

[1] Sergey Antipov, Daniel Broemmelsiek, David Bruhwiler, Dean Edstrom, Elvin Harms, Valery Lebedev, Jerry Leibfritz, Sergei Nagaitsev, Chong-Shik Park, Henryk Piekarczyk, *et al.*, “IOTA (integrable optics test accelera-

tor): facility and experimental beam physics program,” *Journal of Instrumentation* **12**, T03002 (2017).

[2] K Ruisard, HB Komkov, B Beaudoin, I Haber, D Matthew, and T Koeth, “Single-invariant nonlinear

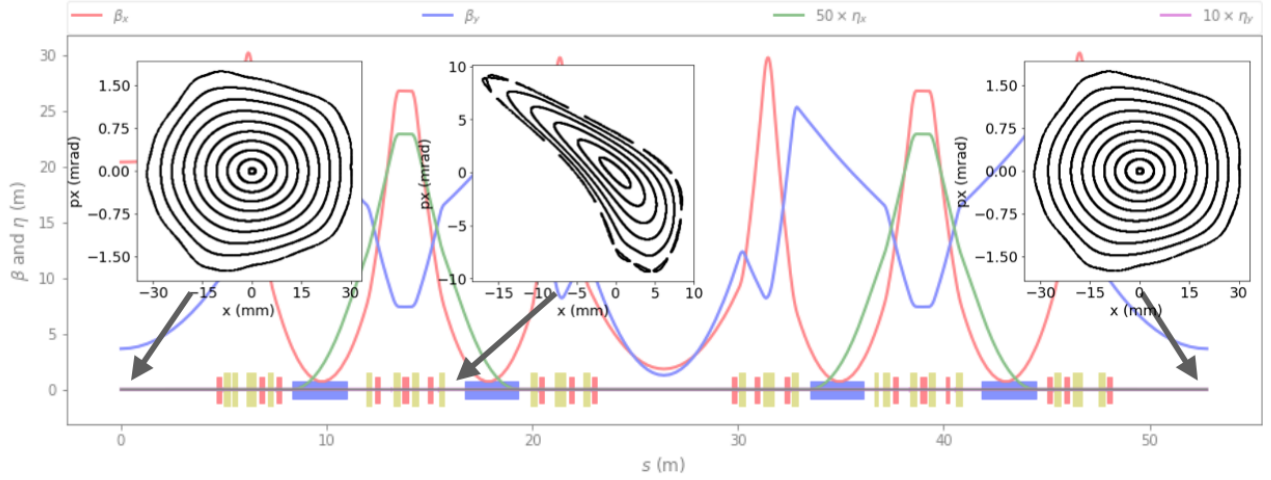


Figure 20. Tori are regular only when observed at the long straight section, but could be distorted at other locations.

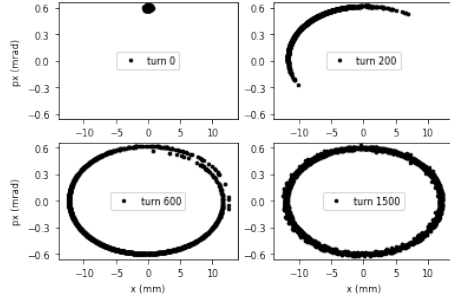


Figure 21. After being kicked, the phase space distribution of the beam spreads from a localized bunch to an annulus which occupies all betatron phases eventually.

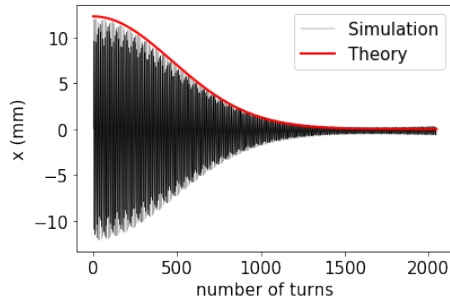


Figure 22. (Colored) After being kicked, the centroid of the beam will show a decaying oscillation. The red line is known as the decoherence factor in ref. [24], and can be used to determine the local tune-shift-with-amplitude.

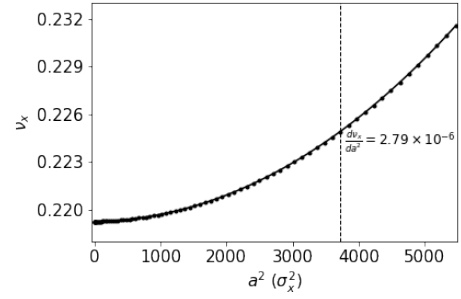


Figure 23. The tune-shift-with-amplitude curve obtained by the single particle tracking simulation. The horizontal axis is measured in the unit of the square of beam size  $\sigma_x^2$ . The local slope at the kicked beam amplitude (at the dashed line) agrees with the decoherence factor computed from the centroid motion in Fig. 22.

Accelerators and Beams **22**, 041601 (2019).

- [3] V Danilov, “Practical solutions for nonlinear accelerator lattice with stable nearly regular motion,” *Physical Review Special Topics-Accelerators and Beams* **11**, 114001 (2008).
- [4] V Danilov and S Nagaitsev, “Nonlinear accelerator lattices with one and two analytic invariants,” *Physical Review Special Topics-Accelerators and Beams* **13**, 084002 (2010).
- [5] Alex J Dragt, “Lie methods for nonlinear dynamics with applications to accelerator physics,” unpublished (2011).

optics for a small electron recirculator,” *Physical Review*

- [6] Li Hua Yu, “Analysis of nonlinear dynamics by square matrix method,” *Physical Review Accelerators and Beams* **20**, 034001 (2017).
- [7] M. Borland, personal communication.
- [8] Yipeng Sun and Michael Borland, “Comparison of Nonlinear Dynamics Optimization Methods for APS-U,” in *2nd North American Particle Accelerator Conference* (2017) p. WEPOB15.
- [9] Joseph Liouville, “Note sur l’intégration des équations différentielles de la dynamique, présentée au bureau des longitudes le 29 juin 1853.” *Journal de Mathématiques pures et appliquées*, 137–138 (1855).
- [10] VI Arnold, “Mathematical Methods of Classical Mechanics, Springer-Verlag, Berlin and New York, 1989,” .
- [11] E.D Courant and H.S Snyder, “Theory of the alternating-gradient synchrotron,” *Annals of Physics* **3**, 1 – 48 (1958).
- [12] Alex J Dragt and John M Finn, “Lie series and invariant functions for analytic symplectic maps,” *Journal of Mathematical Physics* **17**, 2215–2227 (1976).
- [13] A Berz, “Differential algebraic description of beam dynamics to very high orders,” *Part. Accel.* **24**, 109–124 (1988).
- [14] H. Yoshida, “Construction of higher order symplectic integrators,” *Phys. Lett.* **A150**, 262–268 (1990).
- [15] A W Chao, *Lecture Notes on Topics in Accelerator Physics* (SLAC, Stanford, CA, 2002).
- [16] J. Laskar, “Frequency Map Analysis and Particle Accelerators,” in *20th Particle Accelerator Conference (PAC 03)* (2003) p. 378.
- [17] Kalyanmoy Deb, *Multi-Objective Optimization Using Evolutionary Algorithms* (Wiley, 2001).
- [18] DA Edwards and LC Teng, “Parametrization of linear coupled motion in periodic systems,” *IEEE Transactions on nuclear science* **20**, 885–888 (1973).
- [19] BNL, <https://www.bnl.gov/nsls2/project/PDR/>.
- [20] M. Borland, “elegant: A Flexible SDDS-Compliant Code for Accelerator Simulation,” in *Advanced Photon Source LS-287* (2000).
- [21] Laurent Farvacque, N Carmignani, J Chavanne, A Franchi, G Le Bec, S Liuzzo, B Nash, T Perron, P Raimondi, *et al.*, “A low-emittance lattice for the ESRF,” *Proc. IPAC’13*, 79–81 (2013).
- [22] B Riemann and A Streun, “Low emittance lattice design from first principles: Reverse bending and longitudinal gradient bends,” *Physical Review Accelerators and Beams* **22**, 021601 (2019).
- [23] Tong Zhang and Xiaobiao Huang, “Numerical optimization of a low emittance lattice cell,” *Nuclear Instruments and Methods in Physics Research Section A: Accelerators, Spectrometers, Detectors and Associated Equipment* **923**, 55–63 (2019).
- [24] R. E. Meller, A. W. Chao, J. M. Peterson, Stephen G. Peggs, and M. Furman, “Decoherence of Kicked Beams,” *SSC-N-360* (1987).